Supporting Information

Direct Determination of Absolute Absorption Cross Sections at the L-Edge of Dilute Mn Complexes in Solution using a Transmission Flatjet

Markus Kubin[a], Meiyuan Guo[b], Maria Ekimova[c], Michael L. Baker[d], Thomas Kroll[e], Erik Källman[b], Jan Kern[f], Vittal K. Yachandra[f], Junko Yano[f], Erik T. J. Nibbering[c,*], Marcus Lundberg[b,*], Philippe Wernet[a,*]

[a]Institute for Methods and Instrumentation for Synchrotron Radiation Research, Helmholtz-Zentrum Berlin für Materialien und Energie GmbH, 12489 Berlin, Germany.
[b]Department of Chemistry - Ångström Laboratory, Uppsala University, SE-75121 Uppsala, Sweden.
[c]Max-Born-Institut für Nichtlineare Optik und Kurzzeitspektroskopie, 12489 Berlin, Germany.
[d]The School of Chemistry, The University of Manchester at Harwell, Didcot, OX11 OFA, U.K.
[e]Stanford Synchrotron Radiation Lightsource, SLAC National Accelerator Laboratory, Menlo Park, CA 94025, USA.
[f]Molecular Biophysics and Integrated Bioimaging Division, Lawrence Berkeley National Laboratory, Berkeley, CA 94720, USA.

[*]Authors to whom correspondence should be addressed.

Philippe Wernet, Helmholtz-Zentrum Berlin, Albert-Einstein-Str. 15, 12489 Berlin, Germany, Tel: +49 30 806213448, email: wernet@helmholtz-berlin.de.
Marcus Lundberg, Uppsala University, SE-75121 Uppsala, Sweden, Tel: +46-18-4713708, email: marcus.lundberg@kemi.uu.se
Erik T. J. Nibbering, Max-Born-Institut für Nichtlineare Optik und Kurzzeitspektroskopie, 12489 Berlin, Germany. Tel: +49 30 63921477, email: nibberin@mbi-berlin.de

1. Data Analysis and Processing of Transmission Spectra

1.1 Data Processing

All diode current scans have been normalized by the storage ring current of the BESSY II synchrotron. Single outlier data points, deviating by more than 5σ (σ being the local noise) from a local parabolic fit, have been replaced by the local value of the fit function before further processing of the spectrum data. An example is shown in Fig. S1.

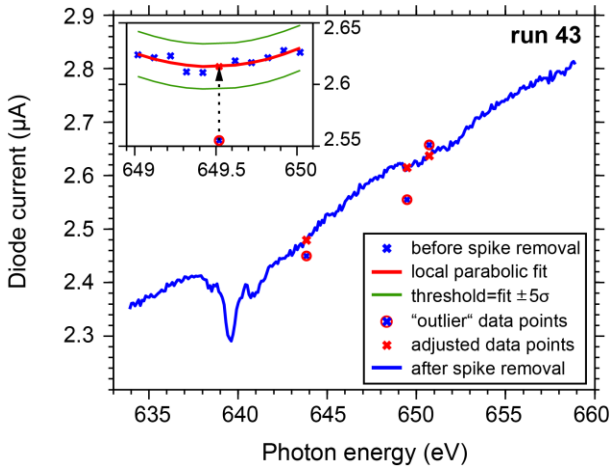

Figure S1. Example for the removal of outlier data points from a single spectrum scan. A local 2nd order polynomial is fitted in a moving window of 1 eV spectral width (centered around the inspected data point, which is excluded from the fit). The local noise level σ is estimated from the fit residuals. The inspected data point is identified as an outlier if it is found outside a margin defined by deviations of ±5σ from the local fit (σ being the local noise level). Outlier data points are removed and replaced by the local fit value (see inset). On average, 3 outlier data points were identified and removed per spectrum scan.

In some cases, the reference signal $I_0(h\nu)$ (with no sample in the beam) was recorded with a monochromator slit size w_0, that was different from the slit size w_s used for the spectrum scan $I_L(h\nu)$ where the sample was inserted in the beam. In these cases the reference signal was proportionally rescaled with a factor w_s/w_0. This procedure was checked for consistency with experimental data, as shown in Fig. S2 for the two slit sizes used in the experiments, 120 µm and 150 µm: Scans 37 and 38 were measured successively under identical experimental conditions, albeit with different slit sizes, 150 µm and 120 µm, respectively. Multiplication of the signal in run 38 by 1.25 = (150µm/120µm) reproduces that of run 37 with good agreement (with a deviation of 1%) in the spectral range relevant for Mn L-edge absorption spectroscopy (630-660 eV).

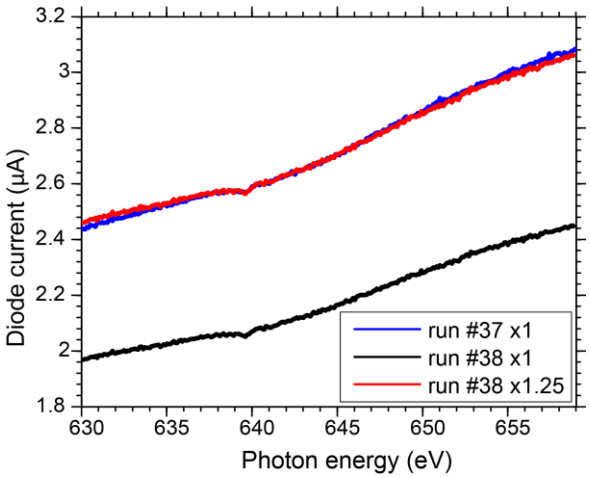

Figure S2. Validity check for rescaling reference scans with the ratio of monochromator slit sizes. Spectrum scans 37 and 38 were measured successively under identical experimental conditions, but with 150 µm and 120 µm monochromator slit sizes, respectively. Rescaling the latter by the ratio of the slit sizes, 1.25 = (150µm/120µm), reproduces the diode signal in the former to a 1% accuracy in the Mn L-edge region.

1.2 Fitting the Sample Thickness with Henke's Tables

In the main paper we point out to have found consistent evidence for an attenuation of the incident x-ray flux increasing over time. This will be further detailed in section 1.3 of this document. In our data analysis, we account for this attenuation with a numerical reduction of the measured incident photon flux (reference scan) by a spectrally constant attenuation factor $Att.$ with $0.4 \leq Att. \leq 1$, so that the corrected photon flux incident on the sample is best described by

$$\Phi_0'(\mathrm{h}\nu) = \Phi_0(\mathrm{h}\nu) * \frac{w_s}{w_0} * Att. \tag{1}$$

Including this attenuation factor, we calculate the experimental transmission $\mathrm{T_L'}(\mathrm{h}\nu)$ and absorbance $A_L'(h\nu)$ (often given in units of optical density, OD) according to the following expressions:

$$\mathrm{T_L'}(\mathrm{h}\nu) = \frac{\Phi_\mathrm{L}(\mathrm{h}\nu)}{\Phi_0'(\mathrm{h}\nu)} = \frac{\Phi_\mathrm{L}(\mathrm{h}\nu)}{\Phi_0(\mathrm{h}\nu) * \frac{w_s}{w_0} * Att.} = \exp\left(-A_L'(h\nu)\right) \tag{2}$$

and

$$A_L'(\mathrm{h}\nu) = -\ln\left(\mathrm{T_L'}(\mathrm{h}\nu)\right) = -\ln\left(\frac{\Phi_L(h\nu)}{\Phi_0(h\nu) * \frac{w_s}{w_0} * Att.}\right) \tag{3}$$

The subscript L denotes the effective sample thickness with respect to the x-ray beam.

In section 1.2.1 of this document, with a few examples we illustrate how the sample thickness is determined by fitting with expected transmission curves, as extracted from Henke's tables (see refs. S1, S2). For these examples, excellent agreement is found for the comparison of experimental and expected transmission curves without including the attenuation factor (keeping *Att.*:=1). Second, in section 1.2.2 of this document we illustrate for another set of spectrum scans the relevance of including this attenuation factor in order to consistently fit the transmission spectra calculated with Henke's tables to our experimental data, where the more conservative approach without this attenuation factor does not explain deviations between the two. We also consistently show that these deviations increased over the time of our experiment.

1.2.1 Fitting Sample Thicknesses with Henke's Tables – the Conservative Approach

In order to retrieve the effective sample thickness L of the transmission flatjet we used the tabulated (spectrally variable) attenuation length $\Lambda(h\nu)$ for pure ethanol together with Beer-Lambert's law (see main paper) to fit the experimental transmission data. For extracting these data from Henke's tables we assumed standard conditions as input parameters to the CXRO data base (refs. S1, S2), namely the sum formula C_2H_6O and mass density ρ=0.789 g/cm³.

Spectrum fits are generally applied only to the non-resonant parts of the spectrum, namely 500-530 eV, 560-638 eV and 658-700 eV, as these parts are accurately described by Henke's tables. Minor oscillations in the experimental spectra at photon energies between 560 eV and 700 eV due to effects of the extended x-ray absorption fine structure (EXAFS) on the O K-edge are small as compared to the large-scale variations of the transmission signal, relevant to our fit approach and will herein be neglected.

An example fit of the effective sample thickness L is shown in Fig. S3 for a transmission spectrum of pure ethanol which was measured over the spectral region of the O K-edge. The experimental data was fitted with eq. (2) ('fit 1'), fixing *Att.*=1. The transmission curve fitted for a sample thickness of 2.44 µm agrees very well with the experimental transmission curve. We note that for this spectrum the fitted value of *Att.* is consistently 1.00 when the parameter is not fixed in the fit procedure ('fit 2').

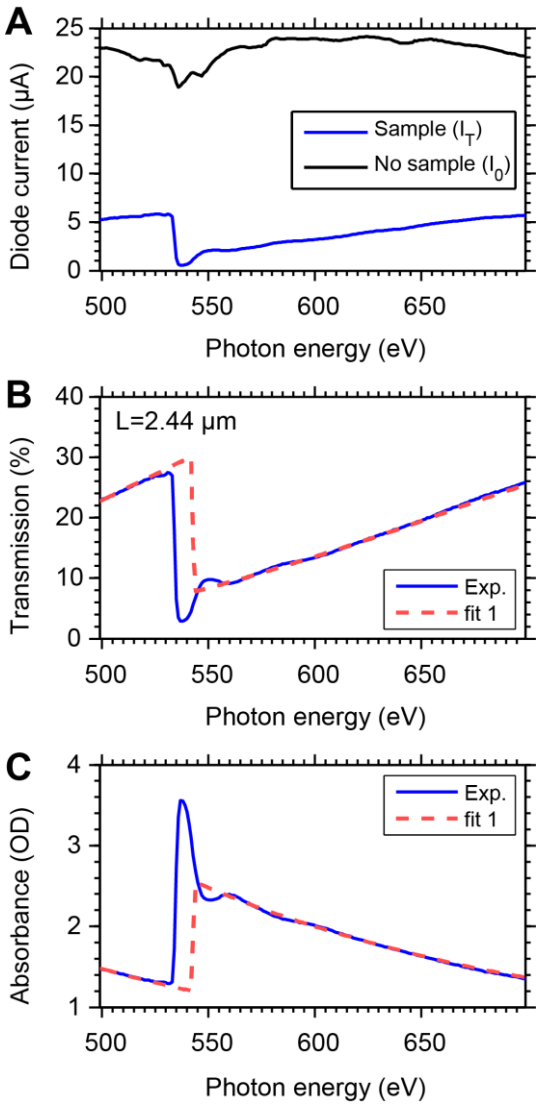

Figure S3. Experimental transmission and absorption spectra of pure ethanol measured at the O K-edge spectral region. The data was acquired in the beginning of the experimental study, where no beam clipping is expected. The data was fitted without including the attenuation factor, as described in the main text of this document. The fit yields a sample thickness of 2.44 μm.

For solution samples with solutes at sufficiently low concentrations one can apply the same fit-approach to determine the sample thickness, using the expected transmission from Henke's tables for the solvent *only*. We checked the validity of this statement for the range of experimental parameters with sample thicknesses around ~3 µm, photon energies from 630 to 660 eV and, in particular, for our low sample concentrations. Neglecting the solute contribution in the transmission, as calculated with Henke's tables, changes the expected transmission by only a small fraction: For our 100 mM, 30 mM and 15 mM solutes, this corresponds to systematic errors of less than 2%, less than 1% and less than 0.5%, respectively. This deviation is negligible with respect to the sample thickness and thus to the absorption cross sections obtained from our fit approach the transmission of the solvent only. This error is small as compared to the statistical variations of absorption cross sections from separate spectrum scans acquired under equal experimental conditions.

One can, thus, determined the sample thickness of Mn solute-containing ethanol samples from a fit with the expected spectral transmission of only the solvent in the non-resonant spectrum range of Mn L-edge spectra, i.e. below 638 eV and above 658 eV.

An exemplary fit is shown in Fig. S4 for the transmission and absorbance of a 30 mM $Mn^{II}(acac)_2$ complex in ethanol solution. In panels (B) and (C) of this figure, the thickness is determined from the fitted absorbance of the solvent (red dotted). The sample thickness fitted with this approach is ~3.10 µm.

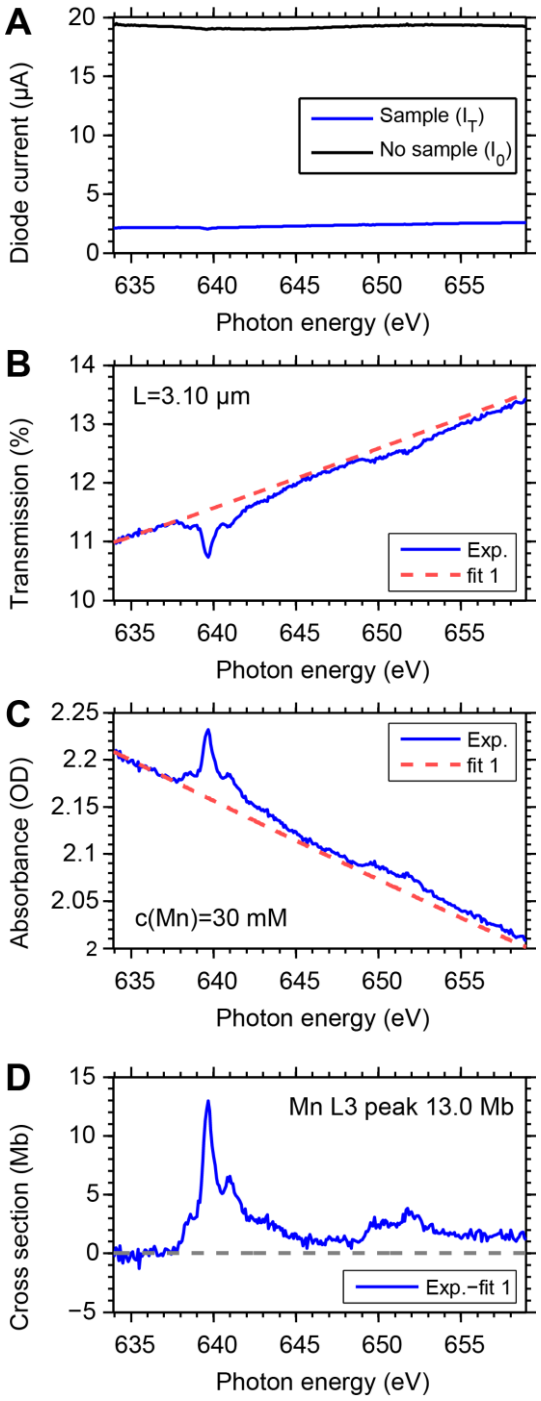

Figure S4. Fitting the experimental transmission and absorption spectra in the Mn L-edge spectral region for a Mn^{II} complex in ethanol. The data was acquired in the beginning of the experimental study, where no beam clipping is expected. The data was fitted without including the attenuation factor, as described in the main text of this document. The fitted sample thickness is 3.10 μm. (D) shows the absorption cross section of the Mn^{II} complex at the Mn $L_{3,2}$-edges, as obtained from the data in (C) after subtraction of the fit, using eq. (4).

From this, we extract the L-edge absorption signal of the Mn complexes (absorbance) $A'_{Mn}(h\nu)$ via subtraction of the fitted curve of the solvent. With the additional information on the sample thickness L and the concentration c or number density n of Mn we retrieve the absorption cross sections $\sigma_{Mn}(h\nu)$, measured in units of [1 Mbarn] = [10^{-22} m²]. In terms of experimental units, this absorption cross section is expressed as follows:

$$\sigma_{Mn}(h\nu)\ [\mathrm{Mbarn}] = 16.61 \times \frac{A'_{L,\ Mn}(h\nu)\ [OD]}{L\ [\mu m] \times c\ \left[\frac{mol}{l}\right]} \qquad (4)$$

Fig. S4 D shows the absorption cross section spectrum of a single $Mn^{II}(acac)_2$ complex. Notably, the positive cross section on the high-energy side of the Mn L-edge spectrum may be interpreted as the 2p absorption edge-jump due to excitations of Mn 2p electrons to the photoionization continuum. However, the quantitative magnitude of this edge-jump is affected with a high uncertainty for most samples and will be omitted in the final analysis, as we discuss in the following paragraph.

1.2.2 Fitting Sample Thicknesses with Henke's Tables – Including Beam Clipping

We find consistent evidence that the incident photon flux transmitted to the interaction region decreases throughout our experiment, which is observed as a mismatch in the slopes of the expected transmission curves with respect to the experimental ones when applying the conservative fit approach ('fit 1') from the previous section. We observe that this mismatch increases throughout the experiment. We explain this observation with a potential optical clipping of the incident x-ray beam. Because our reference scans were taken in the beginning of our experiment, such clipping consistently explains two effects: First, an overestimation of the incident photon flux and, second, a systematic error in the experimental slope in the transmission and absorption curves, if this beam clipping is not accounted for.

We account for this mismatch by including a constant attenuation factor $Att.$ ($0.4 \leq Att. \leq 1$) as introduced with eqns. (1), (2) and (3) in the introduction of section 1.2. In an improved least squares fit, this factor $Att.$ together with the sample thickness L are considered the only two fit parameters. In order to distinguish the two fit approaches, we herein label our improved approach 'fit 2', whereas the conservative approach from the previous section is labelled 'fit 1', which assumes $Att. = 1$.

In Fig. S5 we show the attenuation factor $Att.$, as it decreases from scan to scan throughout the experiment. The most probable reason for this observation is the optical clipping of the incident x-ray beam over time. This may have occurred in the beamline optics itself or in the narrow transmissive tube in the differential pumping stage of the vacuum setup, which may have possibly shifted over time, relative to the x-ray beam axis.

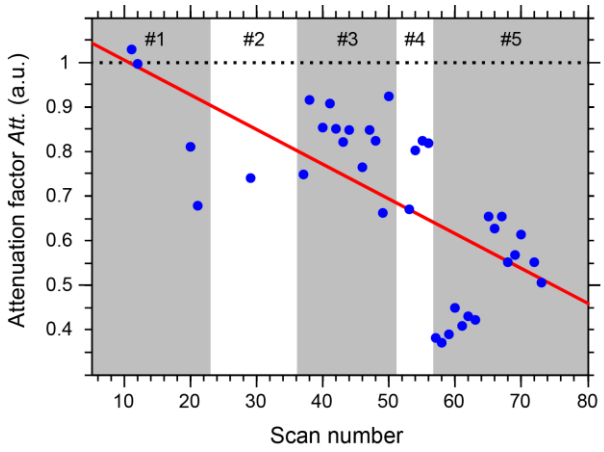

Figure S5. Linear decrease of the effective attenuation factor *Att.* throughout our experimental study, as explained with optical clipping of the incident x-ray beam. The plot shows the fitted factors *Att.* (blue dots, as obtained from 'fit 2') and reveals a decrease from shifts #1 throughout to shift #5. The linear fit (red solid) of these data points emphasizes the decreasing trend. We note that at the start of the experiment the fitted value of *Att.* was unity, as expected.

In Fig. S6 we compare our two fit approaches for a spectrum scan of the O K-edge region of pure ethanol. In Fig. S7 we compare our two fit approaches for a spectrum scan of the Mn L-edge region for a 15 mM $Mn^{III}(acac)_3$ sample dissolved in ethanol. In both figures, the improved fit approach ('fit 2') is plotted in the right columns and resolves the deviation of the transmission curves fitted with 'fit 1' from the experimental curves, as shown in the left columns. In the left column of Fig. S6, the deviation is manifested in a mismatch of the experimental transmission and that expected from 'fit 1' at the low and the high energy sides of the O K-edge jump. This mismatch is not observed in the right column of Fig. S6, where *Att.* is considered a fit parameter. In the Mn L-edge spectral region, as shown in the left column of Fig. S7, the deviation is manifested only in a mismatch of the slopes in the experimental and the expected transmission curves ('fit 1'). This mismatch is not observed with the improved 'fit 2' in the right column of Fig. S7. We note, that the sample thicknesses as resulting from the two approaches 'fit 1' and 'fit 2' differ significantly. These thicknesses are compared in Table S1 (columns 7 and 8). In particular, accurate knowledge of this thickness is crucial for determining the absorption cross section of the studied solutes.

Based on the discussions lined out in this section, we decided to base our analyses of all spectra relevant for the main paper on the improved fit approach, 'fit 2'. The parameters and spectra retrieved from this improved fit approach are used in our final analyses and throughout the main paper.

We note, that for the Mn L-edge spectrum region, our improved fit approach considers the non-resonant regions of the L-edge spectrum scans to be dominated by the absorption characteristics of the solvent, but neglects the fact that the data points on the high energy side of the Mn L-edge spectrum includes information on the absorption cross section due to the 2p absorption edge-jump. We checked that the relative influence of this edge-jump on the sample thickness fitted with the absorption characteristics of only the solvent is negligible. We thus summarize, that with our fit approach we accept losing accurate information on the edge-jump absorption-signal, whereas we significantly improve the accuracy of our information on the sample thickness. For our study of the absolute absorption cross sections, this latter information is most relevant.

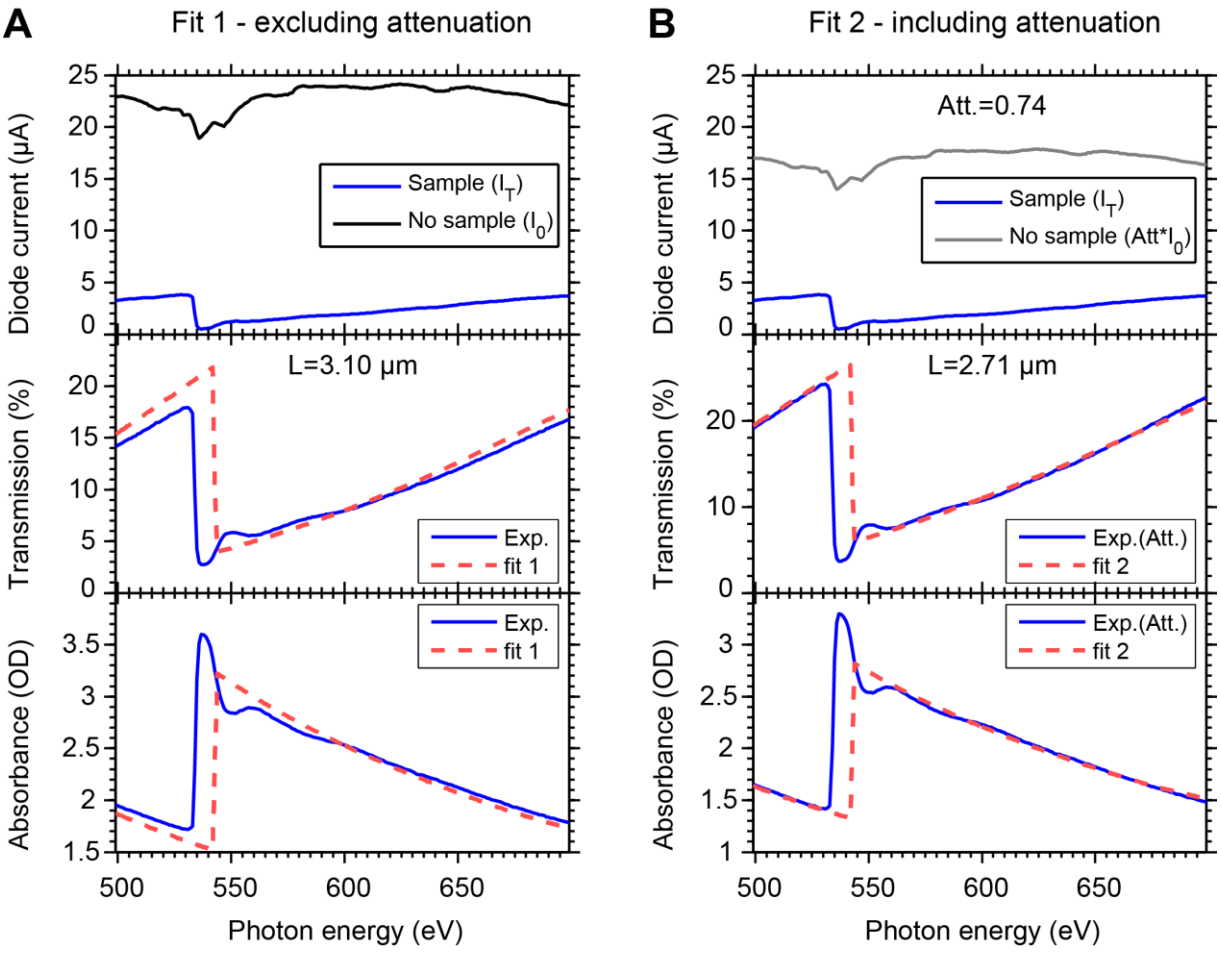

Fig. S6. Comparison of the fit approaches 'fit 1' (A) and 'fit 2' (B) for an O K-edge absorption spectrum, with and without the attenuation factor, respectively. The left column represents the same analysis as shown in Fig. S2, whereas the right column shows this analysis with the additional consideration of optical beam clipping via inclusion of the attenuation factor *Att.*. This attenuation factor, as retrieved from 'fit 2' is $Att. = 0.74$, pointing out to an overestimation of the true photon flux by ~35% in the left column (compare the black and gray curves in the top panels of this figure). The fitted sample thickness from 'fit 2' is L=2.71 µm and is ~14% smaller than that found from 'fit 1'. The fits in the right column to the corrected experimental data show better agreement than those in the left column without this correction.

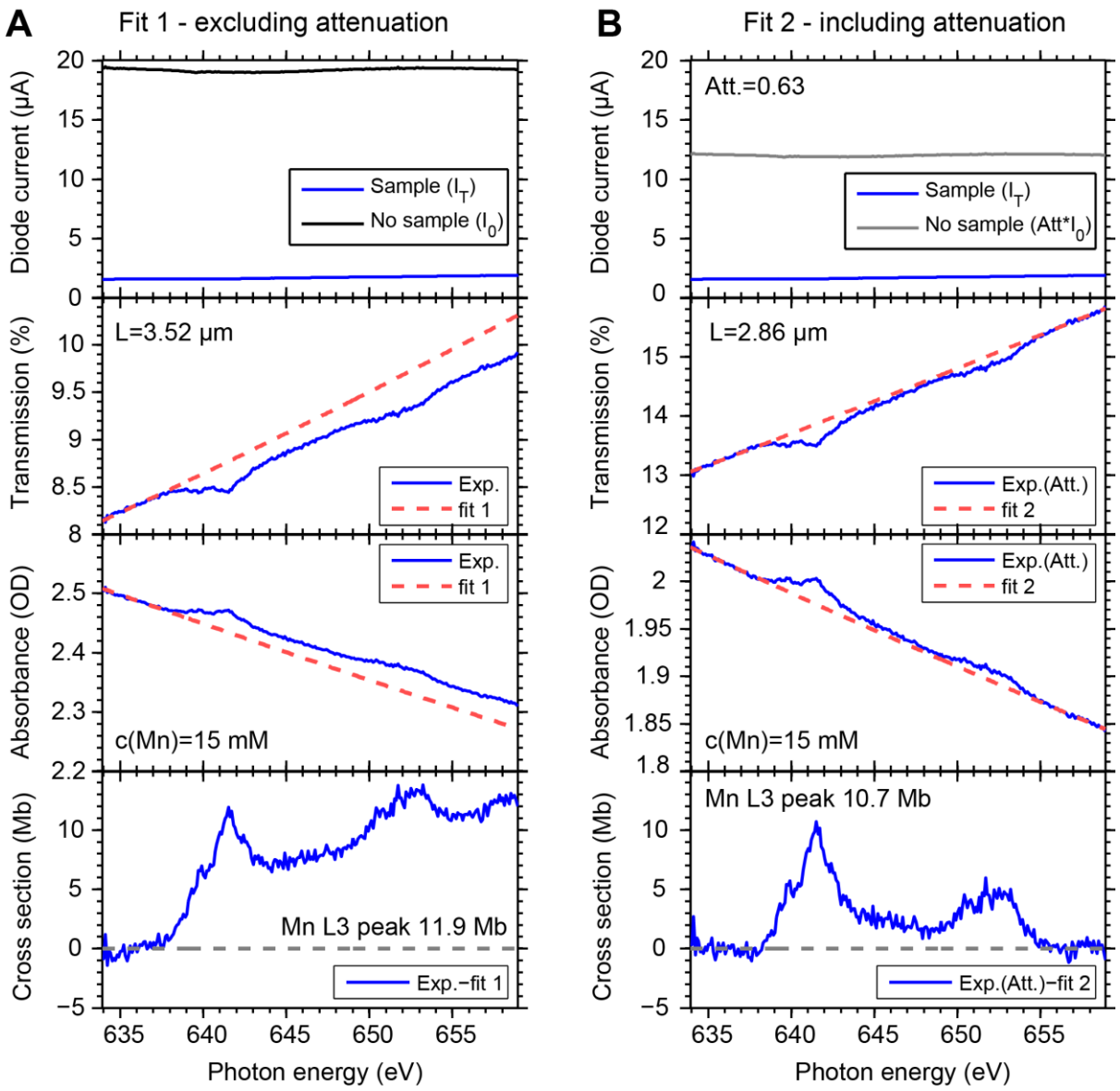

Figure S7. Comparison of the fit approaches 'fit 1' and 'fit 2' for a Mn L-edge absorption spectrum, with and without the attenuation factor, respectively. The left column represents the same analysis as shown in Fig. S3, whereas the right column shows this analysis with the additional consideration of optical beam clipping via inclusion of the attenuation factor *Att.*. The sample thickness from 'fit 2' (with $Att. = 0.63$) is L=2.86 μm and is ~23% smaller than that found from 'fit 1'. Better agreement of the fit with experimental data is found for 'fit 2'.

1.3 Averaging of Spectrum Scans

The final absorption spectra shown in Figs. 3 to 7 of the main paper are averaged from eight successive single-scan spectra of 30 mM $Mn^{II}(acac)_2$ and 13 single-scan spectra of 15 mM $Mn^{III}(acac)_3$ (sample batch A) plus two single-scan spectra of 100 mM $Mn^{III}(acac)_3$ (sample batch B). The single-scan and averaged spectra are shown in Fig. S8.

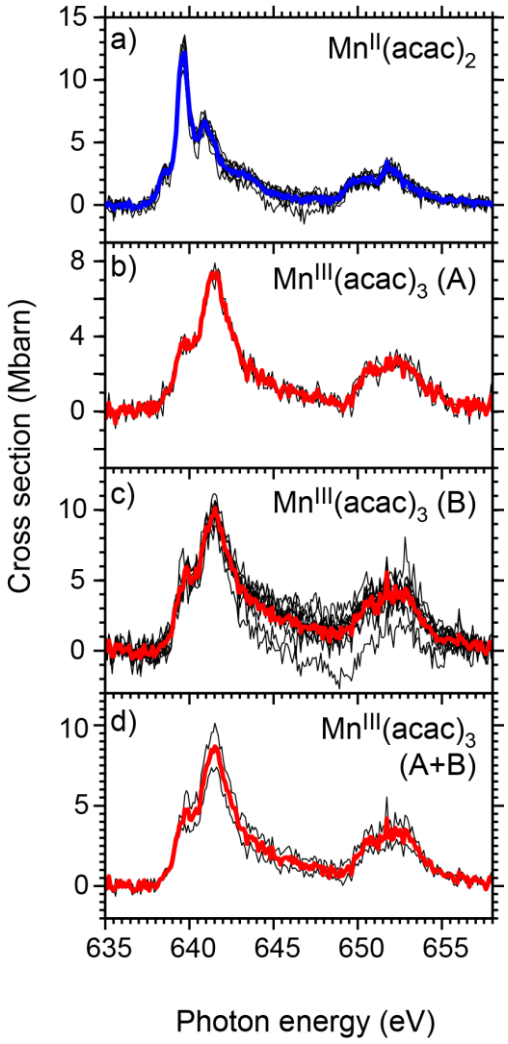

Figure S8. Average absorption spectra (blue and red solid), as averaged from several single spectrum scans (black thin). Panel (a) shows these data for the 30 mM $Mn^{II}(acac)_2$ solution sample in ethanol, panel (b) shows these data for 100 mM $Mn^{III}(acac)_3$ and panel (c) for the 15 mM $Mn^{III}(acac)_3$ solution samples in ethanol. Panel (d) shows the average of the two average spectra shown in panels (c) and (b). The average spectra shown in the main paper are shown in panels (a) and (d).

2. Details on Spectrum Calculations

2.1 Crystal Field Multiplet and Charge Transfer Multiplet Calculations

Table S1. Input parameters for the CFM/CTM spectrum fits to our experimental L-edge XAS of $Mn^{II}(acac)_2$ and $Mn^{III}(acac)_3$. A negative input in O_h symmetry simulates a T_d environment.

	Mn^{2+} CFM	**Mn^{2+} CFM**	**Mn^{2+} CTM**	**Mn^{3+} CFM**	**Mn^{3+} CFM**	**Mn^{3+} CTM**
sim. symmetry	O_h (T_d)	D_{4h}	D_{4h}	O_h	D_{4h}	D_{4h}
10 Dq	-0.6	-0.1678	-0.232	+1.5	+1.845	+1.738
Dt		0.054772	0.024		0.034	0.014
Ds		-0.1567	-0.165		0.291	0.212
Δ_{bb}			2.819			
Δ			2.555			1.758
Q-U			1			1
T_BB_B1g			0.935			
T_BB_A1g			0.935			
T_BB_B2g			0			
T_BB_Eg			0			
T_B1g			0.8			1.2
T_A1g			1.27			1.7
T_B2g			0.8			1.0
T_Eg			1.1			1.0
SOC reduction (core)*		1.0	1.0	1.0	1.0	1.0
SOC reduction (valence)*		1.0	1.0	1.0	1.0	1.0
Lorentzian broadening L_3/L_2 (FWHM) (eV)	0.2 / 0.7	0.2 / 0.7	0.2 / 0.7	0.2 / 0.7	0.2 / 0.7	0.2 / 0.7
Gaussian σ (eV)	0.127	0.127	0.127	0.127	0.127	0.127
T (K)	300	300	300	300	300	300

* The applied reduction of the Slater-Condon parameters for the Fdd, Fpd, Gpd integral values is 0.8 of the Hartree-Fock values. The free-ion values implemented in the CTM4XAS interface consider this reduction factor 0.8 for the Fdd, Fpd, Gpd integral values and are not further reduced.

2.2 Restricted Active Space (RAS) Calculations

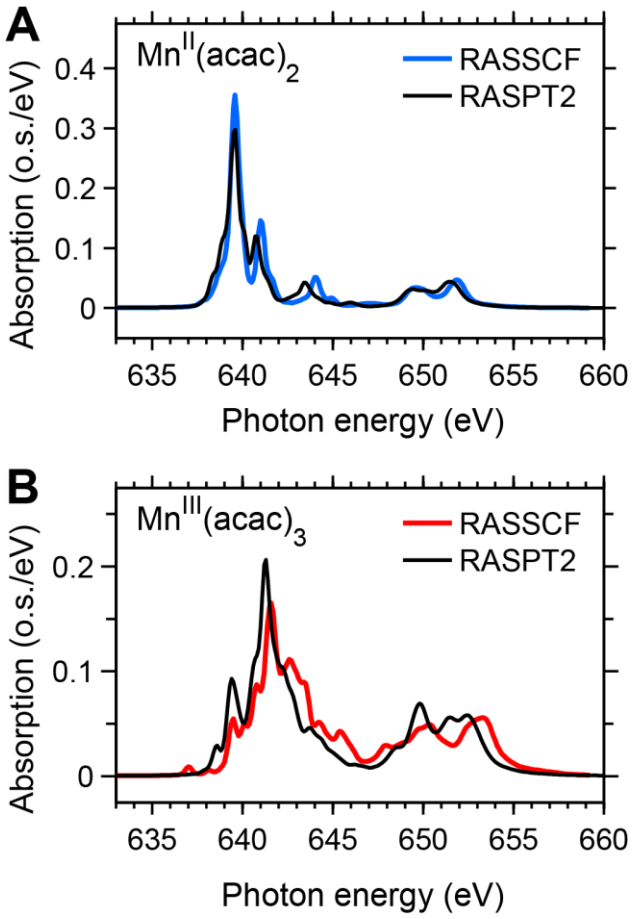

Figure S9. Comparison of RASSCF to RASPT2 spectra calculated at the ANO-RCC-VTZP level for (A) $Mn^{II}(acac)_2$ and (B) $Mn^{III}(acac)_3$. For easy comparison, spectra are given in the same units (oscillator strengths per eV). The RASPT2 spectra are identical with the RAS spectra shown in the main paper. The RASSCF spectra are both shifted by -5.70 eV in order to match the maximum position of the L_3-edge calculated for $Mn^{II}(acac)_2$.

3. Numerical Spectrum Analyses

Table S2. Comparison of experimental and theoretical Mn L_3-edge x-ray absorption cross sections, integral areas and branching ratios for the L-edge absorption spectra of $Mn^{II}(acac)_2$ and $Mn^{III}(acac)_3$, here labelled as Mn^{II} and Mn^{III}, respectively.

Sample	**L_3 Peak Cross Sec. (Mbarn)**	**L_3 Peak Amplitude, Relative (a.u.)**	**L_3 +L_2 Integral value (Mbarn·eV)**	**L_3 +L_2 Integral value, Relative (a.u.)**	**L_3/(L_3+L_2) Branching ratio** *for cutoff energy 647.5 eV*
Exp. Mn^{II}	12.4±1.0	1	41.4±3.3	1	0.72±0.02
Exp. Mn^{III}	8.8±1.9	0.71±0.15	48±11	1.16±0.28	0.66±0.02
RAS Mn^{II}	-	1	-	1	0.78
RAS Mn^{III}	-	0.69	-	1.29	0.65
CFM(O_h) Mn^{II}	-	-	-	-	0.76
CFM(O_h) Mn^{III}	-	-	-	-	0.66
CFM(D_{4h}) Mn^{II}	-	-	-	-	0.76
CFM(D_{4h}) Mn^{III}	-	-	-	-	0.65
CTM(D_{4h}) Mn^{II}	-	-	-	-	0.75
CTM(D_{4h}) Mn^{III}	-	-	-	-	0.67

References of the Supporting Information

S1. Henke, B. L.; Gullikson, E. M.; Davis, J. C., X-Ray Interactions: Photoabsorption, Scattering, Transmission, and Reflection at E = 50-30,000 eV, Z = 1-92. *Atomic Data and Nuclear Data Tables* 1993, *54* (2), 181-342.

S2. CXRO Center for X-ray Optics, X-ray Database (http://henke.lbl.gov/optical_constants/). (accessed 06/01/2017).